

Lawrence Berkeley National Laboratory

LBL Publications

Title

THE NATURE AND ORIGIN OF SLIDING WEAR DEBRIS FROM STEELS

Permalink

<https://escholarship.org/uc/item/7t1779pp>

Author

Salesky, W.J.

Publication Date

1983-02-01

2



Lawrence Berkeley Laboratory

UNIVERSITY OF CALIFORNIA

Materials & Molecular Research Division

RECEIVED
LAWRENCE
BERKELEY LABORATORY

APR 15 1983

LIBRARY AND
DOCUMENTS SECTION

To be presented at the International Conference
on Wear, Reston, VA, April 11-14, 1983

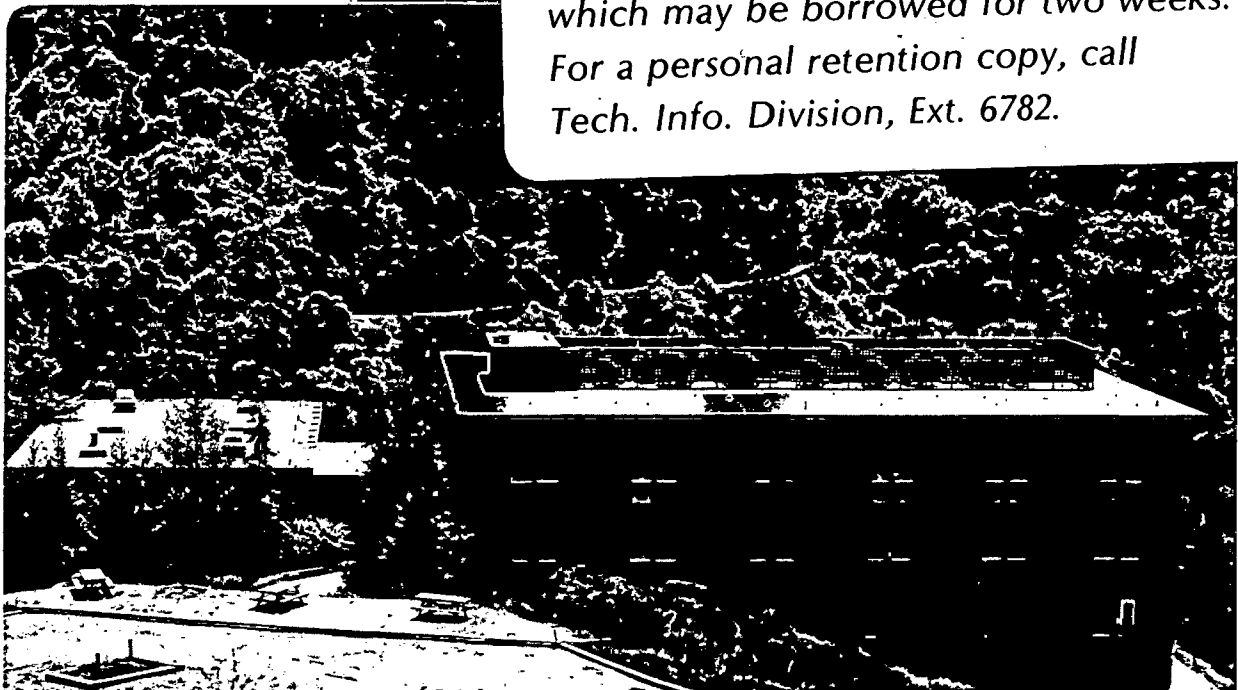
THE NATURE AND ORIGIN OF SLIDING WEAR DEBRIS
FROM STEELS

W.J. Salesky, R.M. Fisher, R.O. Ritchie, and
G. Thomas

February 1983

TWO-WEEK LOAN COPY

*This is a Library Circulating Copy
which may be borrowed for two weeks.
For a personal retention copy, call
Tech. Info. Division, Ext. 6782.*



LBL-15059
2

DISCLAIMER

This document was prepared as an account of work sponsored by the United States Government. While this document is believed to contain correct information, neither the United States Government nor any agency thereof, nor the Regents of the University of California, nor any of their employees, makes any warranty, express or implied, or assumes any legal responsibility for the accuracy, completeness, or usefulness of any information, apparatus, product, or process disclosed, or represents that its use would not infringe privately owned rights. Reference herein to any specific commercial product, process, or service by its trade name, trademark, manufacturer, or otherwise, does not necessarily constitute or imply its endorsement, recommendation, or favoring by the United States Government or any agency thereof, or the Regents of the University of California. The views and opinions of authors expressed herein do not necessarily state or reflect those of the United States Government or any agency thereof or the Regents of the University of California.

**THE NATURE AND ORIGIN OF SLIDING WEAR DEBRIS
FROM STEELS**

**W. J. Salesky, R. M. Fisher, R. O. Ritchie and G. Thomas
Materials and Molecular Research Division
Lawrence Berkeley Laboratory
Department of Materials Science and Mineral Engineering
University of California
Berkeley, California 94720**

ABSTRACT

The mechanism of wear particle formation during unlubricated sliding wear of several carbon and alloy steels has been investigated by scanning (SEM) and transmission electron microscopy (TEM). A detailed study by SEM of individual debris particles has revealed that they are plate-like and typically 200 to 400 nm in thickness. The thinner particles are generally iron oxides except for tests conducted at low temperatures or in inert atmospheres when predominantly metallic particles result. Using SEM automatic image analysis, the mean debris particle width was determined to be 1 to 2 μm . Examination of cross-sections from bulk specimens by TEM revealed a fine dislocation cell structure typical of large strain deformation to a depth of 10 to 50 μm , depending on the material and load. The subsurface cell dimensions and bending of pearlite colonies indicate that the shear strain near to the surface is at least 5. In many instances, a 200 to 300 nm wide zone of lower dislocation density, indicative of recovery, was noted immediately below the surface. Some cracks formed along dislocation cell walls at the boundary of the recovered zone; others were associated with decohesion of particle interfaces or subgrain triple points. Some oxidation then

occurs during separation of the platelet from the parent material as a consequence of the highly pyrophoric nature of thin metal flakes. The sequence of the dry sliding wear process is discussed in light of these considerations.

INTRODUCTION

Inasmuch as wear is not a property of a material, but characteristic of a system, the fundamental factors which determine the rates of sliding wear of metal on metal as a basis for materials design have proved to be very complex to define. Also, the specific nature of worn particles from the wear debris have not been clarified. Various investigators such as Archard (1), Kimura (2), Rigney (3,4), Rosenfield (5,6), Samuels (7), Suh (8,9), and Vingsbo (10,11) have proposed mechanisms for the production of wear particles for metal on metal systems. However, such models have not specifically addressed the fact that in unlubricated sliding wear, especially in ferrous materials, wear debris is predominantly oxide (12). An oxidation mechanism by Quinn (13,14) involves oxide growth on the wearing surface to a critical extent prior to spallation, thereby producing oxide wear debris. Clearly, at high sliding velocities where frictional heating is significant, Quinn's mechanism is plausible. However, in low speed sliding, oxide particles are produced which are several orders of magnitude thicker than the oxide on the wear surface (12). In such circumstances, Quinn's mechanism would not appear to apply and therefore an alternative mechanism to explain the oxidation is necessary.

It was the purpose of this study to characterize the subsurface microstructural changes in pure iron and in several iron

base alloys leading to the creation of wear debris, as well as the specific nature of the debris particles, in order to derive fundamental mechanisms of unlubricated sliding wear including the occurrence of oxide wear particles at low sliding speeds.

EXPERIMENTAL APPROACH

The materials and the heat treatments selected for this study were as follows:

<u>Material</u>	<u>Composition</u>	<u>Heat Treatment</u>	<u>Structure</u>
Ferrovac E	99.999%Fe	800 °C Aust. (1 hour) + Air Cool	Ferrite
AISI 1020	0.1%C/0.5%Mn/ Fe	900 °C Aust. (1 hour) -- 690°C (2 hrs.) + Furnace Cool	Pearlite & Ferrite
AISI 1020	0.1%C/0.5%Mn/ Fe	900 °C Aust. (1 hr.) + Air Cool + 690°C (24 hrs.) + Air Cool	Sphero- dized Carbide + Ferrite
Experi- mental Alloy	3%Cr/2%Mn/ 0.3%C/0.5%Mo/ Fe	1100°C Aust. (1 hr.)+ Oil Quench + 200°C Temper + Air Cool	Lath Marten- site

The majority of wear tests were performed at ambient temperature in air without lubrication on a pin-on-disk wear machine under dead weight loads of 4.9N and 19.6N. The pins traversed on a freshly ground surface of AISI 52100 steel disk in a circular path for a total distance of 750 m.

The amount of pin-wear was monitored and continuously recorded during all tests by measuring the downward displacement with a transducer (LVDT). The volume loss resulting from wear

was also determined by measuring the weight change of the pin. Both methods yielded mutually consistent results.

To investigate the influence of ambient atmosphere on the character of the debris, the testing platform of the wear machine was maintained under positive pressure of dehumidified helium in a clear vinyl enclosure that was pre-dried with heat tape.

The influence of temperature on the character of wear debris, was also investigated by performing some wear tests at -196°C. The test disk was placed in a polyethylene dish containing liquid nitrogen. Once the pin and disk reached a constant temperature, wear tests were conducted under the liquid nitrogen in the same manner as at room temperature.

The wear debris produced during all sliding wear experiments was recovered from the surface of the disk by magnetic techniques. A dry nitrogen (or helium) gas jet was directed across the wear track to ensure that no loose debris remained in the track. After testing, the debris was placed in a dry static-free container pending analysis.

Due to the submicron size of the debris and the tendency of the debris to collect as aggregates, a technique was developed to disperse the debris uniformly over a surface suitable for microscopic and spectroscopic examination (12). The size and shape distribution of the wear debris was determined by automatic image analysis performed on a scanning electron microscope (SEM) using a computer driven quantitative metallography system (15). This system enabled over 300 particles per specimen to be accurately sized and counted in a relatively short time.

Direct measurement of the particle thickness was made by tilting the specimen through large angles (80-90 degrees) so as to observe the particle edge on. This was done in a high resolution SEM.

The debris was also examined by transmission electron microscopy (TEM). Foils suitable for TEM were prepared by mechanically depositing the debris on to the opposite side of holey carbon grid. Carbon was then vapor deposited over the debris to hold them in place. The particles were examined at 100kV, 200kV, and 1000kV. Electron diffraction was employed to elucidate the crystalline structure of the particles.

Selected debris particles on the SEM specimen mount was determined by Auger Electron Spectroscopy (AES) using conventional sputter-depth profiling with Auger ions until the particular 0.5 - 2.0 μm dia. particle disintegrated.

The worn surfaces were examined directly in the SEM and in mounted, polished and etched cross-sections by optical and scanning electron microscopy.

Thin foils for transmission electron microscopy (TEM) were prepared from cross-sections cut from the nickel plated pins. Sections were ground and electropolished via conventional window techniques. Argon ion machining was required to obtain regions at the wear interface sufficiently thin to transmit electrons. This additional step is required because the chemical polishing solution does not attack nickel and iron at the same rate. Details of the specimen preparation technique are given elsewhere

(12,16). Foils were then examined at 100kV in a Philips EM301 and 1000kV electron microscope in order to take advantage of the greater penetrating power at higher voltages (17).

RESULTS AND ANALYSIS

Wear Testing

Representative wear data for unlubricated sliding of the steels are plotted in Fig. 1. Three wear tests were averaged for each datum point. Although considerable scatter occurred (10%) especially with light loads, it was quite apparent that the martensitic structures wear less than either ferritic, pearlitic, or spheroidized structures. Pearlite rubbed with small loads reaches a constant wear rate above that of martensite, yet at higher loads, the wear rate steadily increases such that a constant rate is not reached. The wear rate of ferrite, however, increases approximately linearly with time at all loads. Spheroidized structures exhibit a rate of wear similar to that of ferrite, except that, at small loads, spheroidized steel wears faster. Clearly, microstructure plays a significant role in determining the degree of wear under particular conditions.

The appearance of the worn surface of a Ferrovac E pin is illustrated for several magnifications and tilt angles in Fig. 2. Individual debris particles, a few nm in diameter, as well as aggregates are visible. A layered structure with a thickness spacing of 150-300 nm may be noted in the large central crate.

Wear Debris Analysis

Analysis of hundreds of individual particles by SEM automatic image analysis revealed (Fig. 3) that more than 95% of the particles were less than $4\mu\text{m}$ in width. The particles were

typically plate-like having an average aspect ratio of 1:2. For most of the materials examined, the size distribution peak ranged from 0.5 to 1.0 μm . Notably, the spherodized structures formed a large number of small ($< 1\mu\text{m}$ mean diameter) particles, whereas martensite specimens were observed to form many larger (1.0 to 1.7 μm) particles.

Examination of debris particles at different viewing angles by tilting the specimen in the SEM revealed the debris thickness to be 250-400 nm (2500-4000 \AA). A typical particle tilted on edge, as shown in Fig. 4a-d, appears to be a flat sheet. All of the debris from specimens worn in air or in controlled environments exhibit this plate-like character.

Electron diffraction analysis in the TEM revealed the smaller (thinner) debris particles formed in air be oxide (Fig. 5). The constant concentrations of iron and oxygen as a function of depth, derived from AES sputter profiling experiments, confirmed that many particles formed in air were oxide through their full thickness (Fig. 6). Since atmospheric oxidation results in at most a 10nm oxide surface film thickness, oxide particles 250-400nm thick must have been formed by factors other than ambient environmental exposure.

Wear testing in inert gas atmospheres or at low temperature produces metallic particles. TEM electron diffraction studies revealed that a (001) reflection was typically observed suggesting a preferred orientation texture in debris particles (Fig. 7b). Dark field micrographs using this reflection revealed that

the particles contain a large number of very small dislocation cells with misorientations of several degrees.

Metallography

Cross-sections perpendicular to the wear surface and parallel to the sliding direction indicated the occurrence of extensive subsurface plastic strain and subsurface cracks (marked by arrows) as shown in Fig. 8. The thickest heavily deformed layer was usually found in ferrite structures and there were about 20-30 μm thick.

From measurements of the bending of microstructural features (18) (e.g., grains, grain boundaries, etc.) the shear strain in the heavily deformed region was estimated to exceed a true strain of 4 (Fig. 9). Although the use of banded pearlite aided in the measurement of the plastic strain (Fig. 9a, inset), disturbance of the structure of pearlite colonies made it impossible to define their boundaries to determine the amount of strain within 2 μm of the surface. Since the wear debris is formed within this 2 μm region, its characterization was important.

Well defined dislocation cell structures were commonly observed in TEM cross-sections of the wear surface (Fig. 9b, inset). Similar structures had been observed by previous investigation (19-23). Due to the similarity of rolling and wire drawing textures in BCC materials, estimates were made of the subsurface strain using the data of Embury, Keh, and Fisher (24) to relate the dislocation cell width to degree of strain. Details of the method can be found in Ref. 20. These data together with previous measurements are presented in Fig. 9b and

indicate similar estimates of the sub-surface strain distribution. The plastic shear strain at the worn surface was estimated to exceed 5.5. It should be noted that these strains are far greater than those involved in any conventional mechanical test and further that a corresponding very high strain gradient also develops during the wear testing.

As described above, well defined dislocation structures typical of large strain plastic deformation of metals were observed in TEM for longitudinal (parallel to the sliding direction but perpendicular to the worn surface) cross-sections of ferritic, pearlitic, and spheroidized structures, an example of which is shown in Fig. 10. The dislocation structures within 1 μm of the wear surface ranged from 10-60 nm (100-600 \AA) wide by (80-2000 \AA) long. Sections transverse to the sliding direction revealed the dislocation cells to be equiaxed in section and 10-60nm (100-600 \AA) across. Thus, the dislocation cells tend to have a three-dimensional plate-like character.

The relative misorientation across cell boundaries was determined for a number of adjacent cells at various points within the deformed layer in both ferrite and pearlite wear specimens. In most instances, a small selected area diffraction aperture was centered on a particular boundary and the relative misorientation between the several overlapping patterns was estimated from the displacement of the centers of the Ewald spheres. Dark field imaging was used to relate a particular cell to its diffraction pattern. In a few cases, microdiffraction patterns were obtained in the Scanning Transmission Electron Microscope (STEM) from a series of adjacent cells.

The results showed that misorientations near to the surface were often as large as 15° and decreased to 1° at the inner limit of the deformed layer, i.e., an inverse correlation with cell width. Although a systematic study was not carried out, the misorientation appears to approximate a lattice rotation increasing successively from the innermost cell (Heilman, Clark and Rigney have studied this in detail for the case of copper (25). Little difference in the magnitude of the misorientation was noted between cells in the recovered zone.

Since lath martensite is already similar to a heavily deformed metal in its initial state, it was difficult to separate plastic deformation from transformation structures except for shape changes. The martensite lath was observed to neck down from an initial width of $0.5 \mu\text{m}$ (26,27) to less than $0.05 \mu\text{m}$ near the wear interface (Fig. 11). Dislocation cells $0.025 \mu\text{m}$ wide were observed within the laths adjacent to the surface.

Immediately beneath the wear interface in worn ferritic and pearlitic steels, the dislocation cell size was observed to be approximately 60 nm (600 \AA) wide by 80 nm (800 \AA) long (Fig. 12). This region, however, only extended $0.2\text{--}0.3 \mu\text{m}$ from the surface (Fig. 12b). In the underlying region, the dislocation cell width was smaller, $10\text{--}30 \text{ nm}$ ($100\text{--}300 \text{ \AA}$), and longer $200\text{--}300 \text{ nm}$ ($2000\text{--}3000 \text{ \AA}$). The regions immediately beneath the surface were suspected to have undergone recovery as the result of sliding wear. Cracks appear to have formed near the boundary of the recovered zone and the underlying heavily dislocated layer as indicated by arrows in Fig. 12b. The cracks appear to form along the cell boundaries, consistent with the SEM observations indicating crack

formation in the heavily deformed layer along features aligned parallel to the surface.

This is consistent with other observations of subsurface wear cracks along dislocation cell walls. An apparent example of a wear particle of the early stage of formation is shown in the TEM of a cross-section (Fig. 13a). Energy dispersive X-ray analysis was used to confirm the location of the interface. The long arrow denotes the sliding direction and the iron-nickel plate interface. A crack was observed to have formed along the dislocation cell boundary as denoted by the arrows. The particle soon to be formed was denoted by "FE". Note that the thickness of the feature is equivalent to the recovered zone width as well as the typical wear particle thickness. Also note the dislocation cell structure within the "particle" is similar to that of the recovered zone in Fig. 12.

In contrast, crack initiation in the spherodized steel was observed to be associated with carbide particles as indicated in Fig. 13b. Matrix decohesion and crack formation between carbides were observed to be the principal modes of initiation. Thus the TEM and the SEM observations demonstrate that cracks may initiate near particles or dislocation cell boundaries depending on the microstructure of the steel being tested.

DISCUSSION

Based on extensive electron microscope and diffraction analyses of wear debris, and examination of near surface cross-sections of the corresponding worn pins in several steels, the principal features of unlubricated sliding wear appear to be as follows:

(1) The debris consists of plate-like metallic or oxide particles, the size of which is an inverse function of the applied load. The particles become partially oxidized after separation with the degree of oxidation dependent on their thickness and on the nature of the ambient temperature and environment during wear rate testing.

(2) A highly deformed subsurface layer, of a thickness depending on the material and applied load is formed near to the surface with shear strains exceeding 5. Some recovery of the dislocation cell structure is evident to a depth of 0.2 to 0.4 μm .

(3) Subsurface cracks appear to be associated to second phase particles, dislocation cell walls and triple junctions, occurring principally at the boundary between the heavily deformed and recovered zones.

These observations, which bear on the mechanism of sliding wear, are discussed in the plausible sequence of the debris formation. We first considered the deformation strain and recovery in the immediate vicinity of the wear surface.

Deformation Strain and Recovery

During wear rate measurements, the steel test pins are subjected to intervals of rather large shear forces due to friction against the rotating steel disk. The resulting subsurface deformation strain appears to be a dominant factor in wear. Since the wearing surface will work-harden with repeated straining, the region of deformation will extend below the surface to a distance depending upon the applied load, and flow stress of the material (Fig. 9).

Since essentially plane strain conditions prevail with a stress state near the surface of compression and cyclic shear, the dislocation cell structures established by plastic deformation will become increasingly sheet-like as they near the surface (Fig. 10). Their thickness provides a measure of the minimum strain as a function of distance. As discussed, TEM observations showed a reduced dislocation density and cell dimensions suggestive of recovery very near to the surface (Fig. 12). Dynamic recovery is to be expected in this region in view of the very large plastic strain that has occurred as well as the high strain rate and local heating that occurs during the intermittent asperity contacts. The extent of dynamic recovery depends on the material and microstructure as well as strain density and temperature (28). Relatively pure iron, i.e., free of precipitates and dissolved elements to pin dislocations, can recover rather readily. As reported by Emburg, Keh, and Fisher (24), and Langford and Cohen (29) an important consequence of recovery is a disintegration of some cell boundaries at a critical strain value so that the average cell thickness maintains a constant value independent of strain.

A further consequence of recovery is an abrupt change in stored energy, i.e., strain density, near to the surface as illustrated schematically in Fig. 14. A steep strain gradient, such as that indicated in the sketch, and the corresponding internal stresses that result, will result in a tensile component perpendicular to the surface, which clearly has some bearing on the nature of crack initiation, as outlined below.

Crack Initiation and Propagation

The formation of wear debris clearly require subsurface crack nucleation and propagation in that the small particles (Figs. 8 and 13a) can flake off from the surface (30). There are a number of possible mechanisms for crack initiation which are primarily related to the microstructure of the material under test and the effects of the interaction of that microstructure with the very severe plastic strain that is encountered in wear. These are illustrated schematically in Fig. 15 and have been subdivided into mechanisms pertaining to microstructures where particles are important or less important. With respect to the non-particle induced crack initiation mechanisms, one very likely mechanism is where sliding along cell walls can lead to the formation of triple point cracks at cell boundary intersections (Fig. 15a). The mode of strain required to generate such triple point cracks is not known, but by analogy to the formation of wedge cracks during high temperature creep testing where substantial grain boundary sliding occurs, it is clear that such a crack initiation mechanism would be promoted by large shear strains and a large strain discontinuity (which produces a tensile stress across the boundary). As shown in Fig. 14, such conditions are met at the interface between the heavily dislocated and recovered zones, which is exactly where the TEM observations indicate that cracks are formed (Figs. 12 and 13a).

Another possible crack initiation mechanism in the absence of particles is illustrated in Fig. 15b. In this case, dislocation accumulation in the cell wall and the corresponding increase in misorientation reaches a point where boundary decohesion can

be envisaged through the formation of super-dislocations in the very high angle tilt boundary. For a misorientation of 15° in such cell walls, the dislocation spacing in the boundary need only be of the order of 4 Burgers vectors. Observations suggest that this type of decohesion boundary will occur where extremely high residual strain gradients occur, again inferring the crack initiation should preferentially occur at the interface between the heavily dislocated (unrecovered) and recovered zones, as seen experimentally in Figs. 12 and 13a.

Mechanisms for subsurface wear crack formation in the presence of particles, e.g., for spherodized structures, are illustrated in Fig. 15c and d, together with experimental TEM observations in Fig. 13b,c. Two mechanisms are envisaged and both involve particles in the form of carbides or inclusions where voids are created either by cracking of the particle or decohesion at the particle matrix interface. For isolated particles in region of intense shear strain, the process of void formation will be similar to that in the cone portion of a uniaxial tensile cup-and-cone fracture in that the void will elongate by shear of the matrix at the forward and trailing edge of the particle (Fig. 15c). For closely spaced pairs of non-deformable particles in a deforming matrix subjected to shear, the incompatibility of strain between the matrix and particles will induce a void connecting the particles. This is illustrated schematically in Fig. 15d, and has been discussed in detail elsewhere (31). Cracks of both types are readily observed in the case of the spherodized steel samples, as shown in Fig. 13b,c.

The various mechanisms for subsurface wear crack initiation discussed above would suggest that wear cracks initiate below the surface at some level of critical strain at a point comparable with the interface between the recovered and unrecovered layers where the strain gradients are highest (Figs. 12-14). The subsequent propagation of such cracks is currently unclear since the stress and deformation fields below a wearing surface are still uncertain. However, the repeated passage of asperities on the sliding surface will result in the accumulation of large cyclic shear strains, and it is conceivable that subsequent crack propagation occurs by fatigue in Mode II shear (plus compression). Recent analyses by Suh and co-workers (32) of the complex stress state below a wearing surface, however, have suggested the presence of a tensile component in the wake of a slider, and this tension may act to aid the Mode II propagation or conversely allow the cracks to propagate in Mode I.

Debris Particle Formation and Oxidation

The specific details of the final stages of debris particle formation are difficult to prescribe because of the uncertain stress state and surface topography. Clearly the subsurface crack breaks out to the surface and the particle flakes off after local asperity contact with those on the rotating disk.

Electron diffraction and Auger analyses of debris particles (Figs. 5 to 7) revealed that they are partially or fully oxidized depending on their thickness and the testing temperature and environment. Exposure of iron or steel to air at room temperature results in the formation of a 5-10 nm (50-100 Å) film of Fe_3O_4 in a few days. The much thicker oxide thickness observed for

wear debris particles implies that they were heated to above 500° C for a few seconds. The dimensions of debris particles, typically 1 x 2 x 0.3 μm , corresponds to a specific surface area of more than 1.5 $\mu\text{m}^2/\text{gm}$. Metal particles with such a high specific surface area are highly pyrophoric (33). So it is expected that the exothermic heat of oxidation can lead to spontaneous combustion as, for example, sparks from a grinding wheel. The final oxide film thickness depends on the temperature when the particle is exposed to air (34). The oxide thickness observed for debris particles indicates an initial temperature of about 400° C (35). The dislocation structure and diffraction pattern of the more oxidized debris particles (Fig. 5) indicates a substantial amount of recovery and even incipient recrystallization in some cases. This is consistent with heating to 500-600° C for a few seconds.

Based on these arguments, it is apparent that, for the environments studied,, the role of oxidation in the low sliding speed wear process is not a dominant factor, as such oxidation occurs after wear particle formation. This is to be contrasted with Quinn's original model (13,14) for wear in oxidizing environments where oxide films on the wearing surfaces were considered to grow to some critical thickness prior to spallation.

SUMMARY

Large shear forces imposed by repeated contact with the harder surface result in very large shear strains near the surface of 5-6 or more. Cracks develop at different critical strains for different features in the microstructure, i.e., single or clusters of inclusions or cell boundaries or junctions as illustrated in Fig. 15. Dynamic recovery may also occur in

the surface layer resulting in the annihilation of redundant dislocation in the cell walls and the occasional dislocations within the cells. The latter recovery (or in some cases recrystallization) produces a large strain discontinuity at the boundary between the recovered and heavily dislocated layers, thus providing a preferential site for crack initiation.

Exothermal oxidation of the particle momentarily heated by friction to 400 °C results in partial or complete oxidation of the wear particles after their formation.

ACKNOWLEDGEMENTS

This work was supported by the Director, Office of Energy Research, Office of Basic Energy Sciences, Materials Science Division of the United States Department of Energy under Contract No. DE-AC03-76SF00098.

The assistance of Don Jurica, Simon Kwok and members of the LBL staff is gratefully acknowledged.

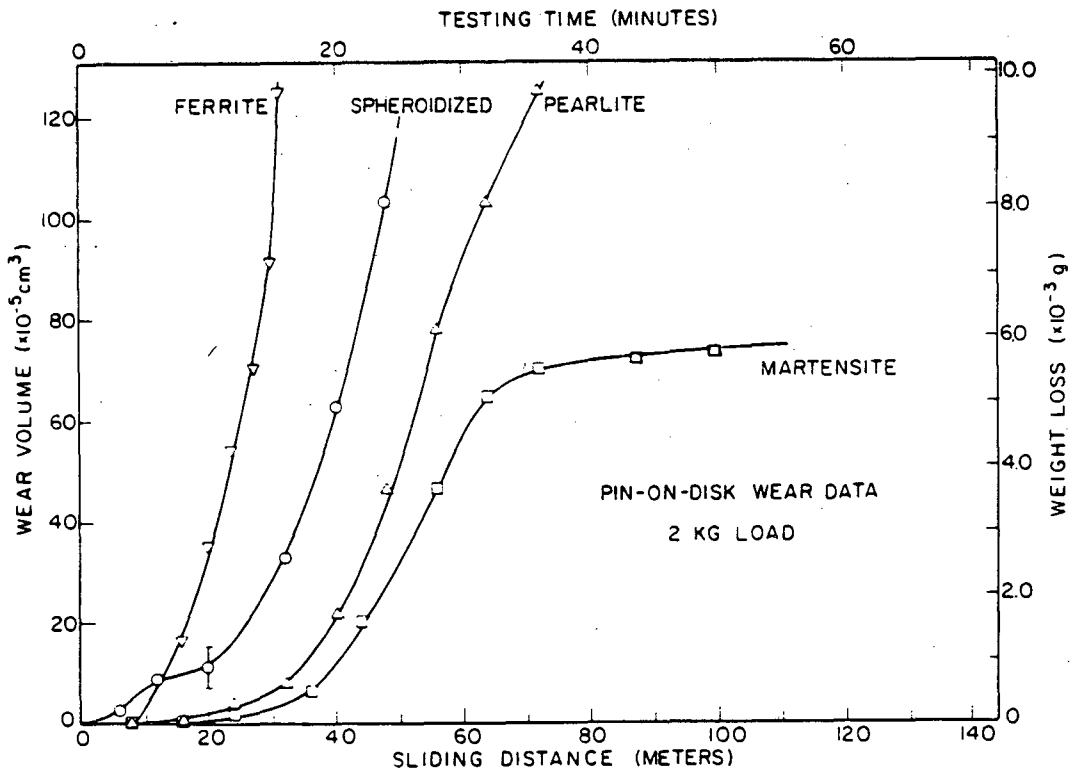
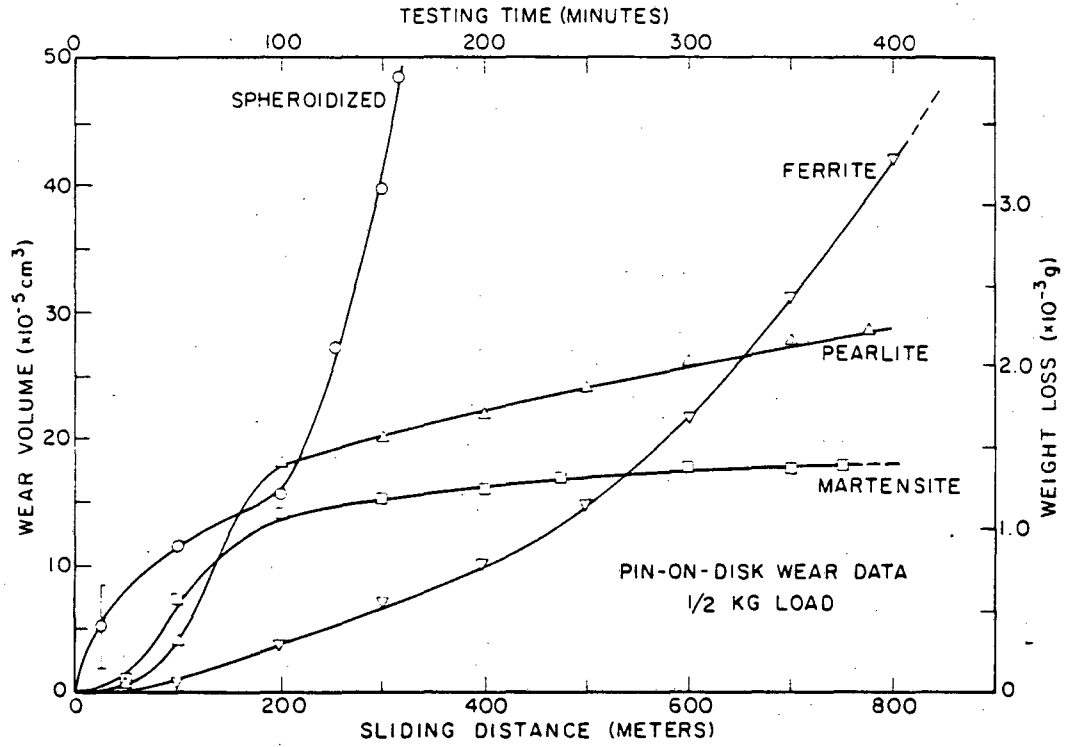
Thanks are due to A. Szirmae, J. W. Conway, and J. R. Kelly of U.S. Steel, Monroeville, PA for assistance with the automatic image analysis and debris particle specimen preparation procedures.

REFERENCES

1. J. F. Archard, "Single Contacts and Multiple Encounters," J. Appl. Phys., 52, 1420-1425 (1961).
2. Y. Kimura, "An Interpretation of Wear as a Fatigue Process," Proc. of the JSLE-ASLE Intl. Conf., Tokyo, Elsevier, 67-73, 1975.
3. J. P. Hirth and D. A. Rigney, "Crystal Plasticity and the Deformation Theory of Wear," Wear, 39, 131-141 (1976).
4. J. P. Hirth and D. A. Rigney, "Microstructural Models for Friction and Wear," Proc. 4th Intl. Strength of Metals and Alloys Conf., Aachen, W. Germany, 1483-1502, Aug. 1979
5. A. R. Rosenfield, "Wear and Fracture Mechanics," in Fundamentals of Friction and Wear of Materials, ASM, Metals Park, OH, 221-233, (1981).
6. A. R. Rosenfield, "A Dislocation Theory Approach to Wear," Wear, 72, 97-103, (1981)
7. L. E. Samuels and E. D. Doyle, "Mechanism in Wear," Wear of Materials II, ASME, N.Y., 1-10, (1979).
8. N. P. Suh, "The Delamination Theory," Wear, 25, 111-124, (1973).
9. N. P. Suh, et al., "The Delamination Theory of Wear," Wear, 44, 1-145, (1977).
10. O. Vingsbo, "Wear and Wear Mechanisms," Wear of Materials II, ASME, N.Y., 620-635, (1979).
11. O. Vingsbo and S. Hogmark, "Wear of Steels," Wear of Materials II, ASME, N.Y., 373-408, (1979).
12. W. J. Salesky, "On the Fundamentals of Sliding Wear in Steels," Ph.D. Dissertation, U.C. Berkeley, Dec. 1982.

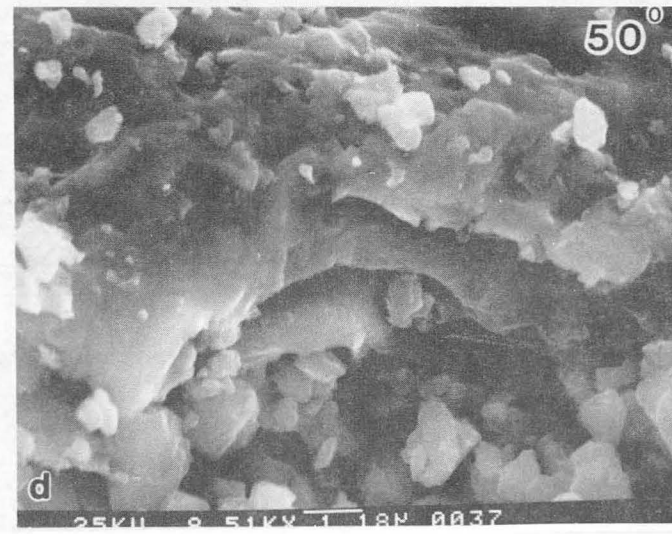
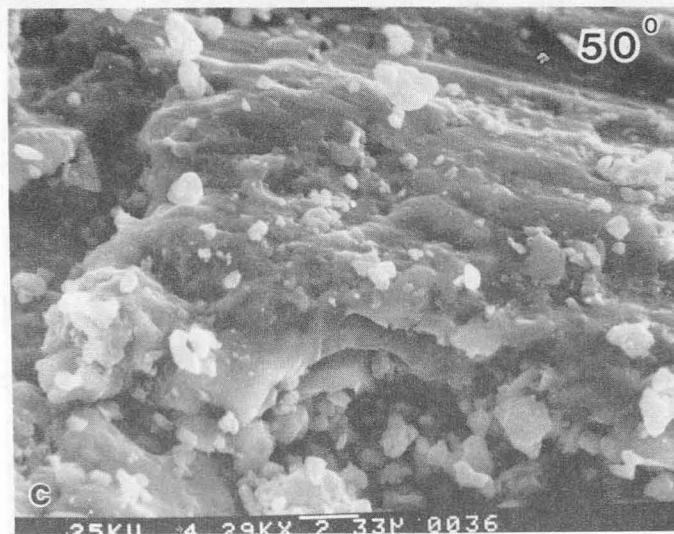
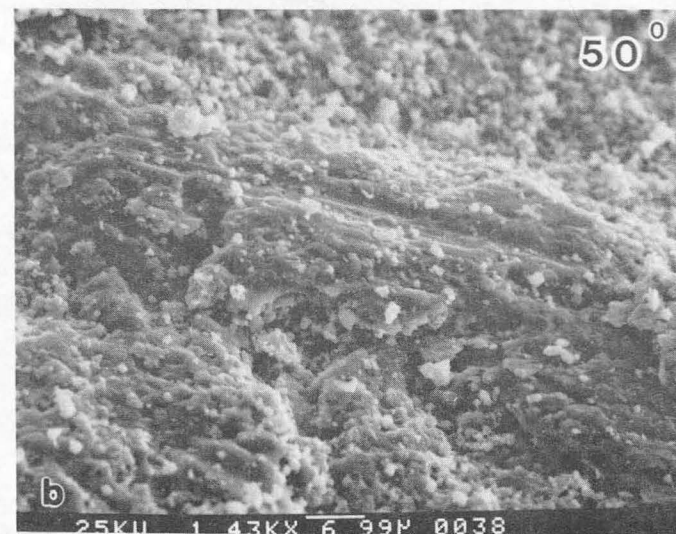
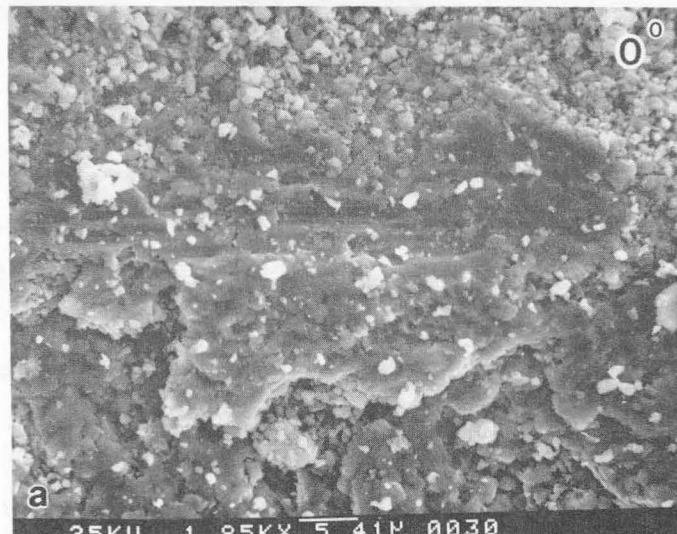
13. T. F. J. Quinn, "Role of Oxidation in the Mild Wear of Steels," Brit. J. Appl. Phys., 13, 33-37, (1962).
14. T. F. J. Quinn, "A Review of Oxidational Wear," Proc. Intl. Conf. on Wear of Materials I, ASME, N.Y., 110-117, (1977).
15. R. J. Lee, W. A. Spitzig, J. F. Kelly and R. M. Fisher, "Quantitative Metallography by Computer-Controlled Scanning Electron Microscopy," Journal of Metals, V33-3, 20-25, (1981).
16. W. J. Salesky, "Wear and Fracture Surface Examination in TEM," EMSA, Aug. 1982.
17. G. Thomas and M. Goringe, Transmission Electron Microscopy of Materials, Wiley, 1979.
18. J. Dautzenberg and J. Zatt, "Quantitative Determination of Deformation by Sliding Wear," Wear, 23, 9-19, (1973).
19. K. Nakajima and Y. Mizutari; Wear, 13, 283 (1969).
20. J. A. B. Van Dijck; Wear, 42, 109, (1977).
21. I. I. Graubar and J.V. Skoinin; Wear, Vol. 51, 327, (1978).
22. J. H. Dautzenberg; Wear, Vol. 60, 401, (1980).
23. D. A. Rigney and W. A. Glaeser, "The Significance of Near Surface Microstructure in the Wear Process," First Intl. Conf. on Wear of Materials, St. Louis, MO, ASME, 41-45, (1977); also in Wear, 46 241, (1978).
24. J. D. Embury, A.S. Keh, and R. M. Fisher, "Substructural Strengthening in Materials Subjected to Large Strains," AIME Trans., 236, 1252-1260, (1966).
25. P. Heilmann, W. A. T. Clark, and D. A. Rigney, "Orientation Determination of Subsurface Cells Generated by Sliding," Private Communication, (1982).

26. B. V. N. Rao and G. Thomas, "Structure-Property Relations and the Design of Fe-4Cr-C Base Structural Steels for High Strength and Toughness," Met. Trans. A, 11A, 441-457, (1980).
27. M. Sarikaya, "Crystallography of Lath Martensite and Stabilization of Retained Austenite," Ph.D. Thesis, U. C. Berkeley, June 1982.
28. J. D. Embury, L. J. Cuddy, and R. M. Fisher, Unpublished Data.
29. G. L. Langford and M. Cohen, "Microstructural Analysis by High Voltage Electron Diffractions of Severely Drawn Iron Wires," Met. Trans. A, 6A, 901-910, (1975).
30. S. Jahanmir and N. P. Suh, "Mechanisms of Subsurface Void Nucleation in Delamination Wear," AIME Trans., 236, 17-38, (1966).
31. T. Goldenberg, T.D. Lee and J.P. Hirth, "Ductile Fracture of U-Notched Bend Specimens of Spheroidized AISI 1095 Steel", Met. Trans A, 9A, 1663-1671, (1978).
32. N. P. Suh et al., "The Delamination Theory of Wear," Elsevier Sequoia, Sausanne, (1977).
33. J. P. Evans, W. Borland, and P. G. Mardon, "Pyrophoricity of Fine Metal Powders," Powd. Met., 1, 17-21, (1976).
34. G. P. Huffman and F.E. Huggins, "Applications of Mossbauer Spectroscopy in the Steel Industry," Advances in Chemistry, 194, Amer. Chem. Soc., Washington, D. C., (1980).
35. R. T. Spurr, "Temperatures Reached by Sliding Thermocouples, "Wear, 61, 175-182, (1980).



XBL 826-5947A

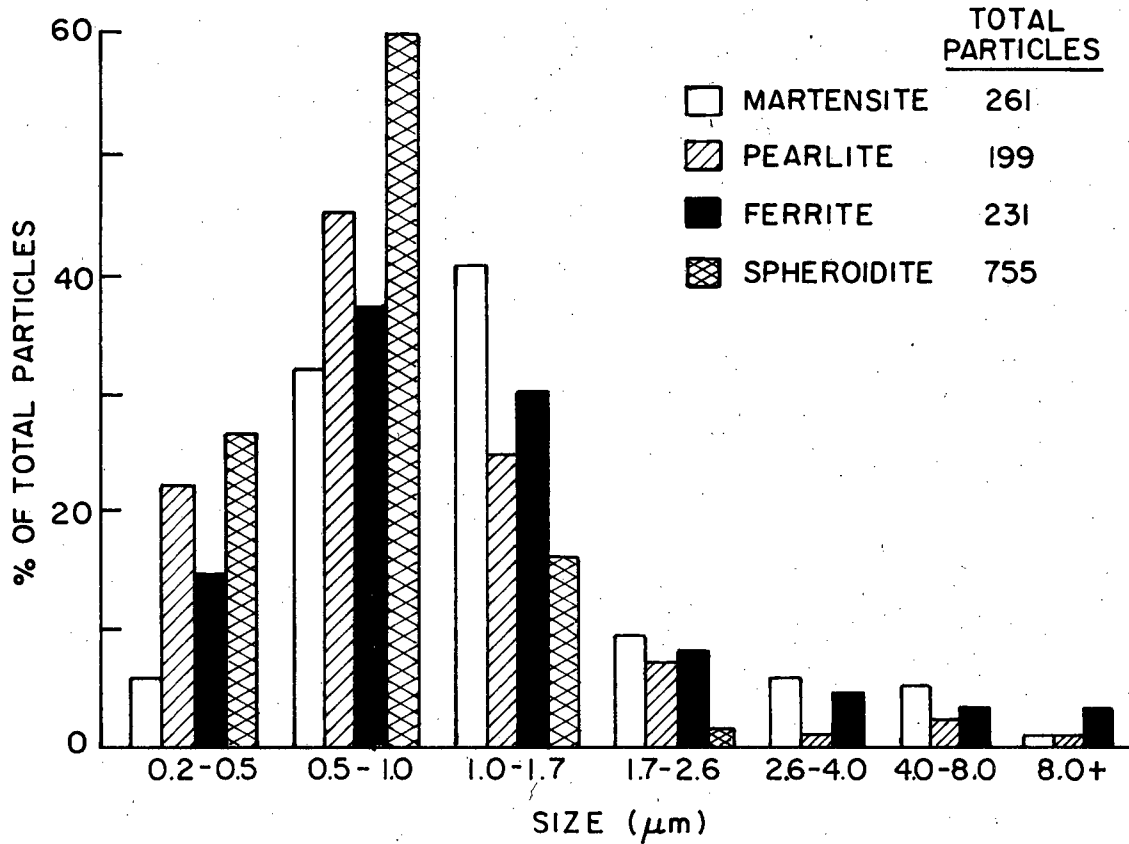
Figure 1: Total pin on disk wear versus sliding distance for several steel microstructures. a) 0.5 kg load b) 2.0 kg load.



XBB 826-5042

Figure 2: Representative SEM micrographs showing appearance of surface craters and debris particles. a) Typical area on the worn pin b) area in (a) after tilting 50° c) Enlargement of (b) d) enlargement of (c) showing that the layered nature of the worn surface is comparable to the debris thickness (150-300nm).

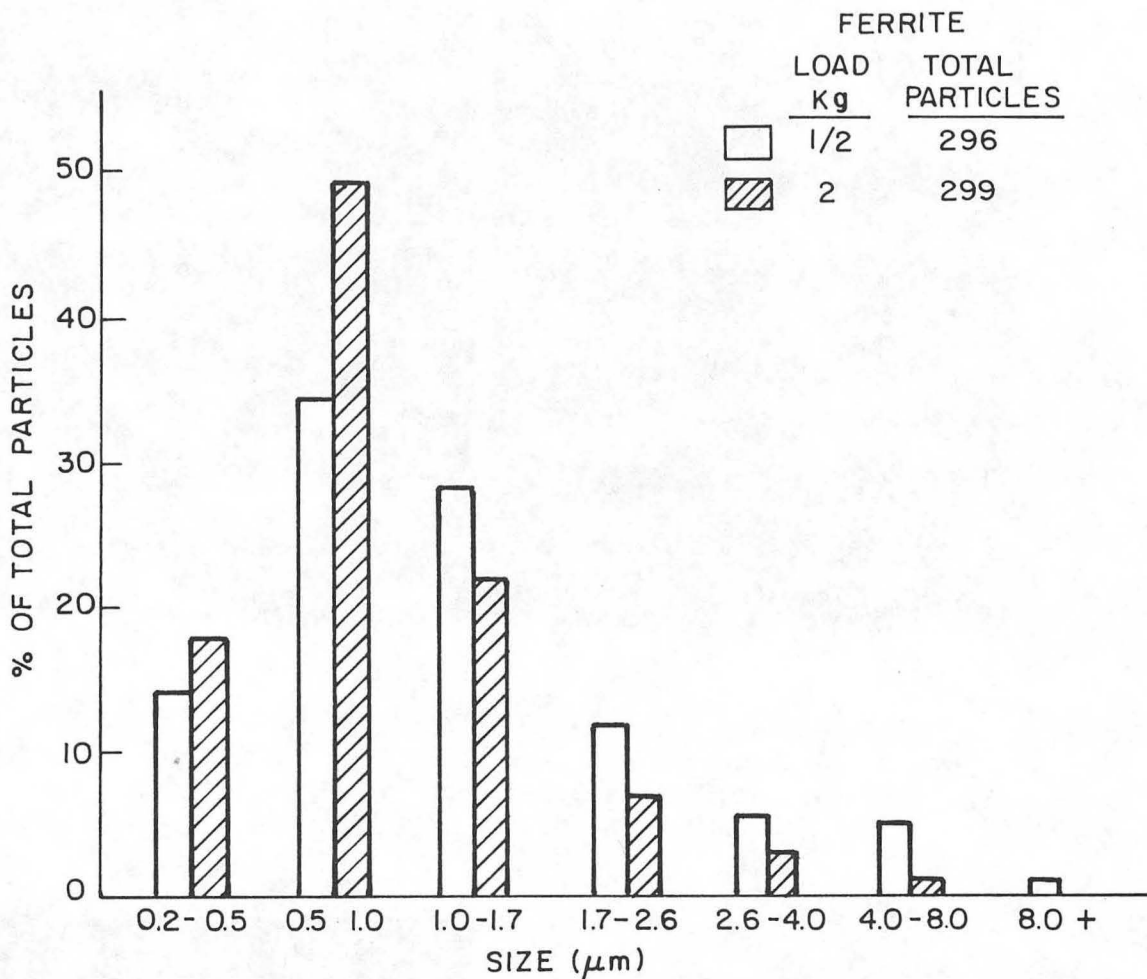
AUTOMATIC IMAGE ANALYSIS
INFLUENCE OF STRUCTURE
(1/2 Kg LOAD P.O.D.)



XBL 822-5147A

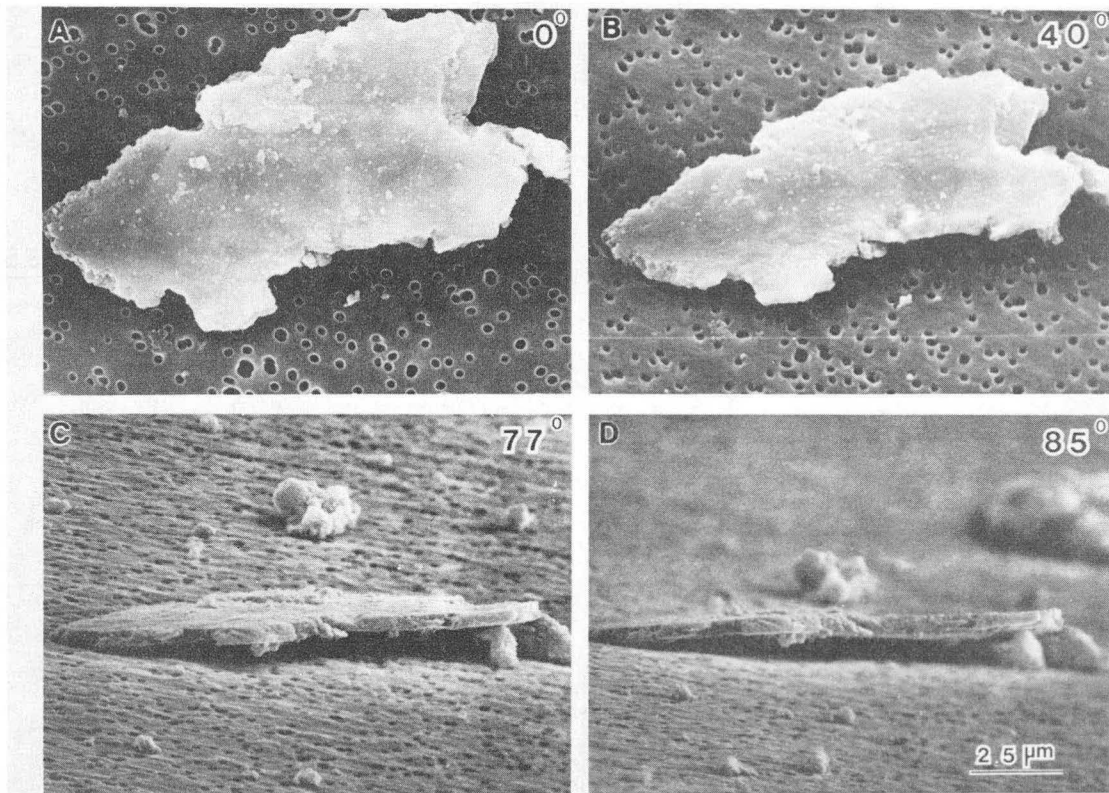
Figure 3: Histogram of particle sizes obtained by computer controlled electron microscopy. a) influence of microstructure b) influence of load

AUTOMATIC IMAGE ANALYSIS INFLUENCE OF LOAD



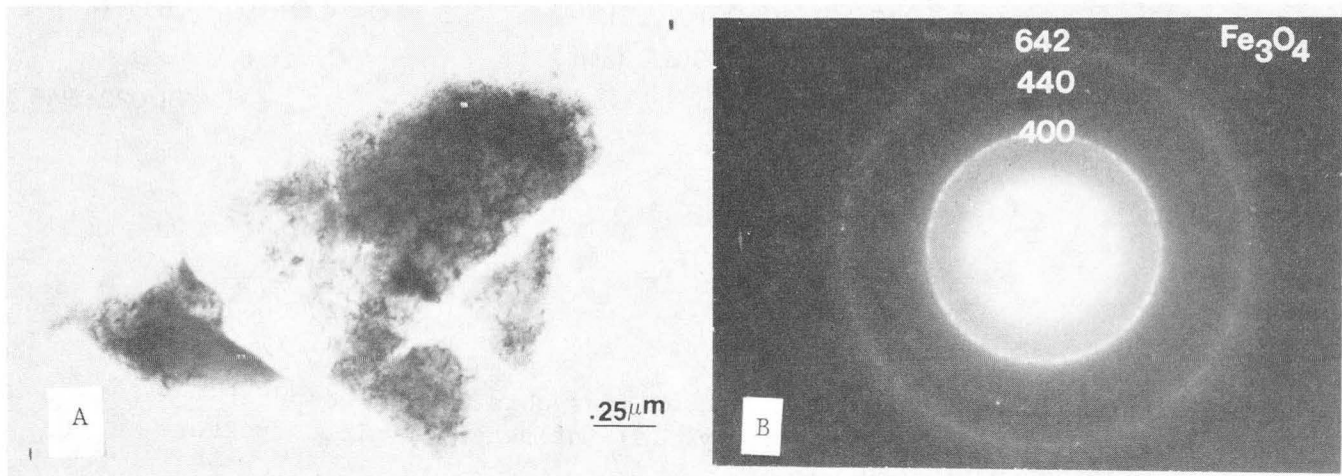
XBL 822-5148

Figure 3: Histogram of particle sizes obtained by computer controlled electron microscopy. a) influence of microstructure
b) influence of load



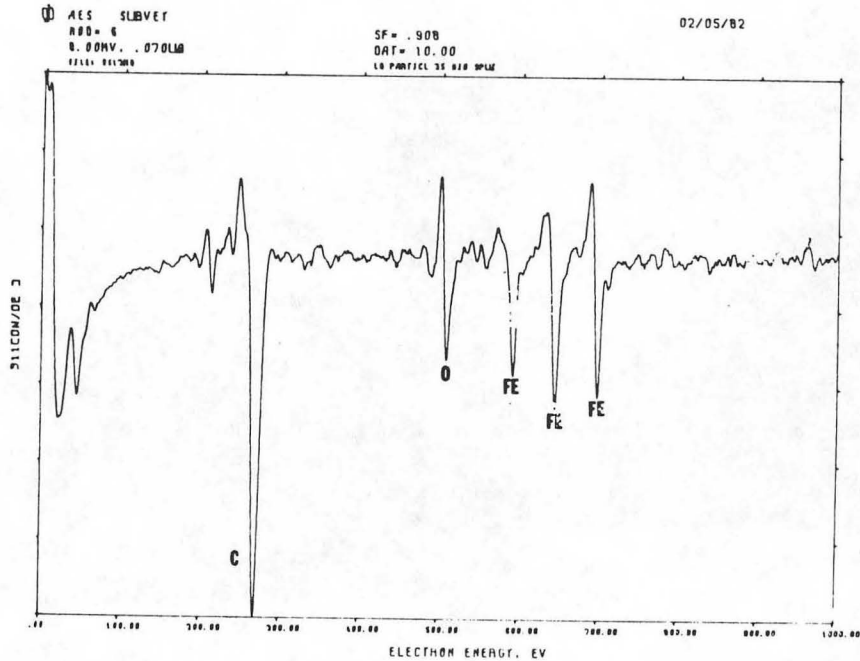
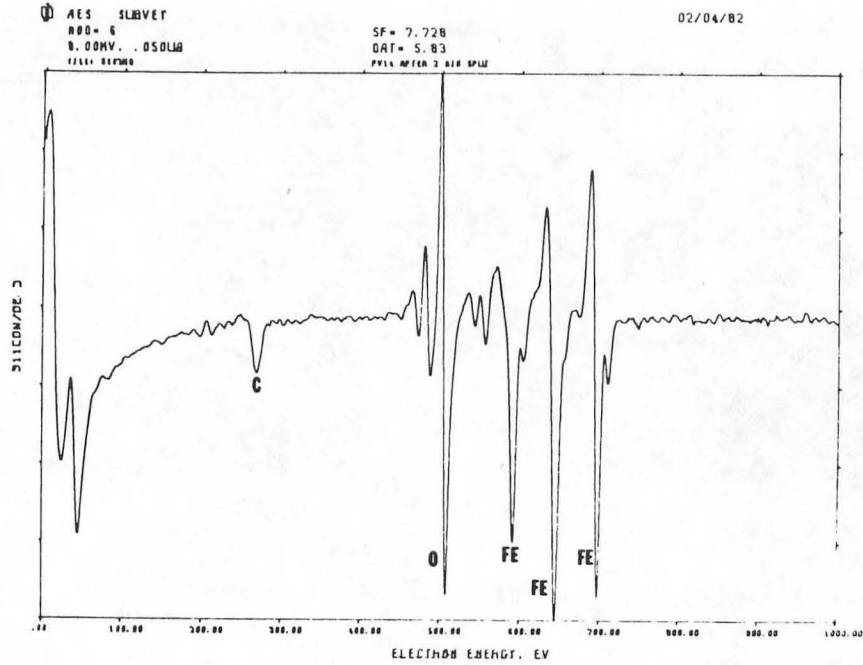
XBB 826-5754A

Figure 4: Typical ferrite wear debris examined in the SEM at oblique angles to reveal its plate-like character. The thickness measured in (d) is 300-400nm.



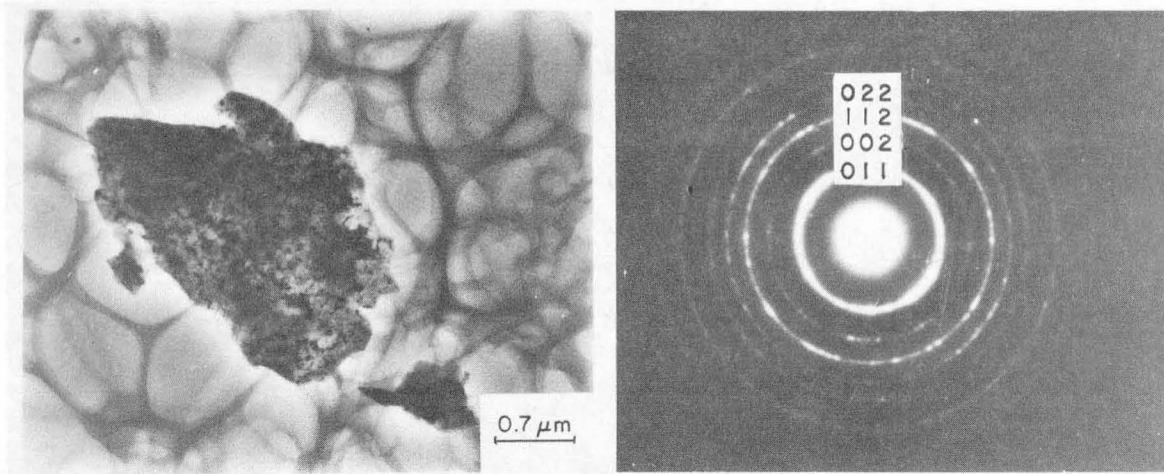
XBB 823-2872

Figure 5: TEM micrograph A and selected area diffraction pattern B showing that small particles are fully oxidized to Fe₃O₄.



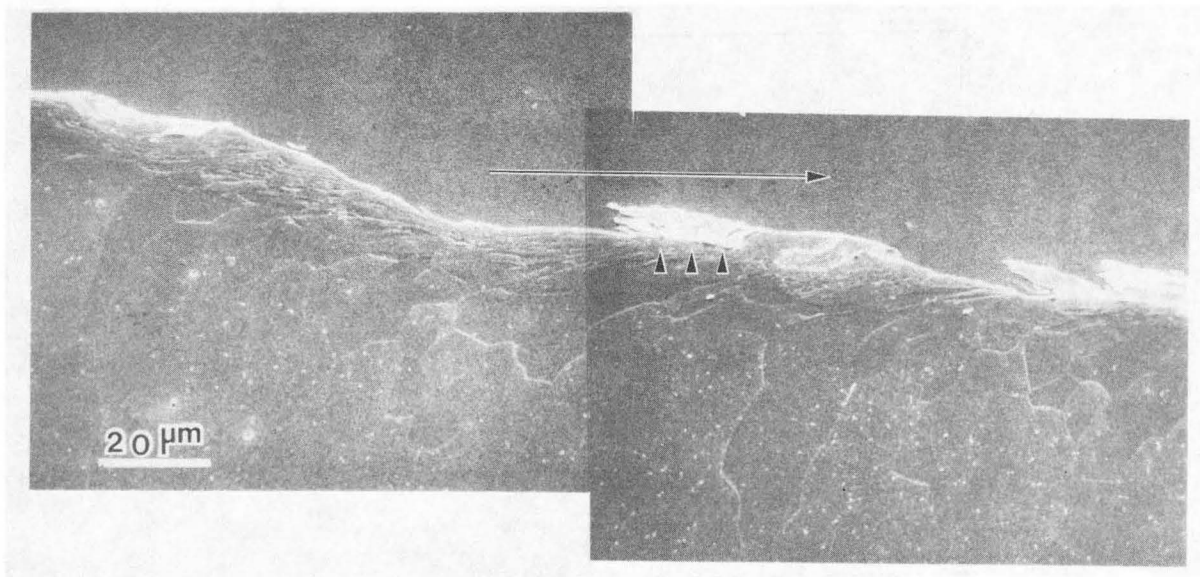
XBL 824-8843

Figure 6: Auger Spectroscopy data from debris formed in air
a) After 2 minutes sputtering the iron oxygen stoichiometry revealed the surface to be hematite. b) Survey after 20 minutes sputter, the oxide appears to be magnetite. The large carbon peak is due to the polycarbonate substrate.



XBB 827-6395A

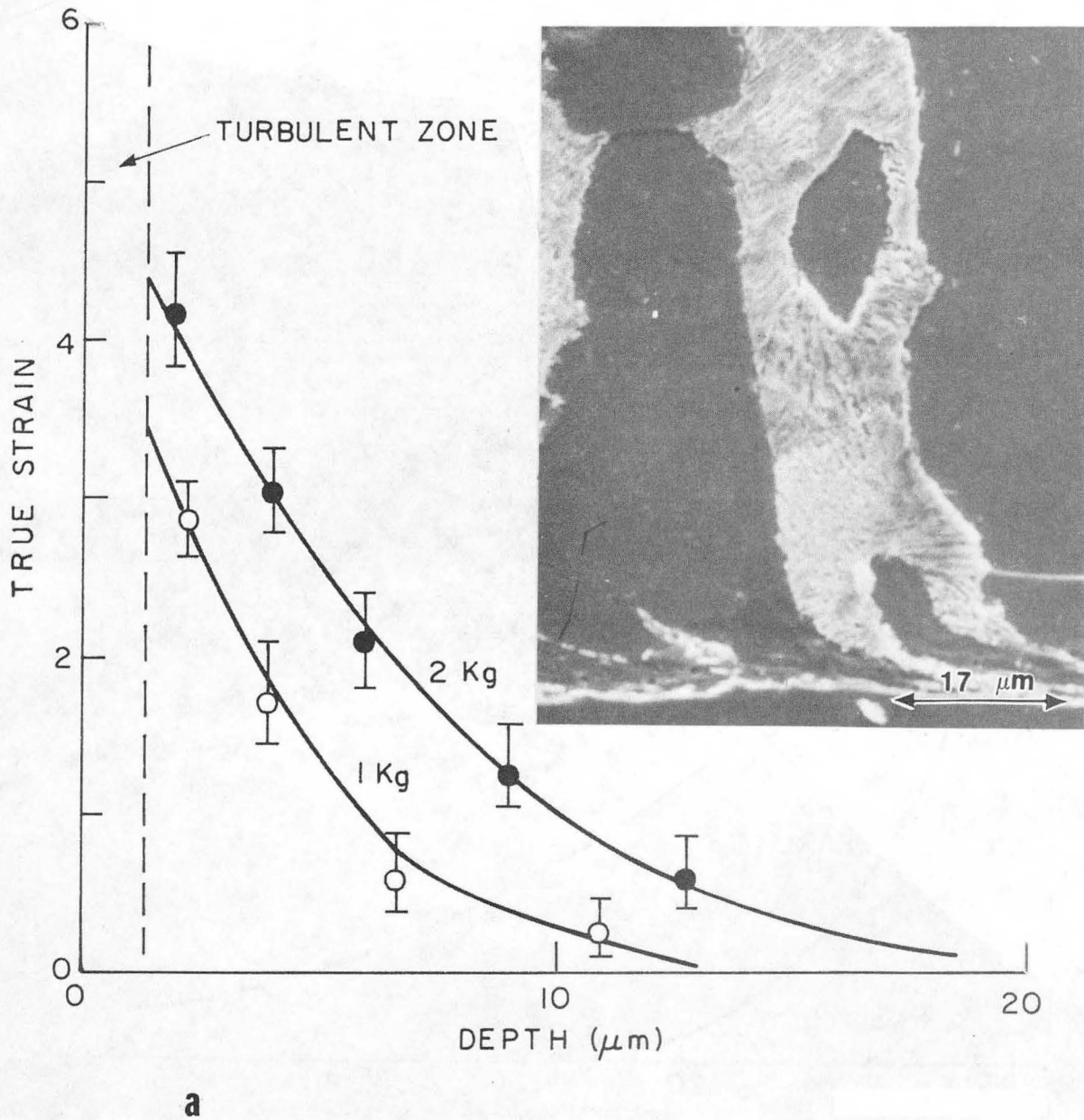
Figure 7: TEM micrographs. a) Wear debris formed in helium atmosphere. b) SAD of the debris in (a) reveals a wholly metallic structure. Note the intense broad (011) reflection indicating extremely fine slightly misoriented cells are present.



XBB 817-5978A

Figure 8: SEM micrograph. Plastic replica of a cross section of a nickel plated ferritic iron. Notice deformation of grains into sliding direction (arrowed). The deformed zone extends 14-19 microns from the surface. Subsurface cracks parallel to the wear surface are shown by arrow heads.

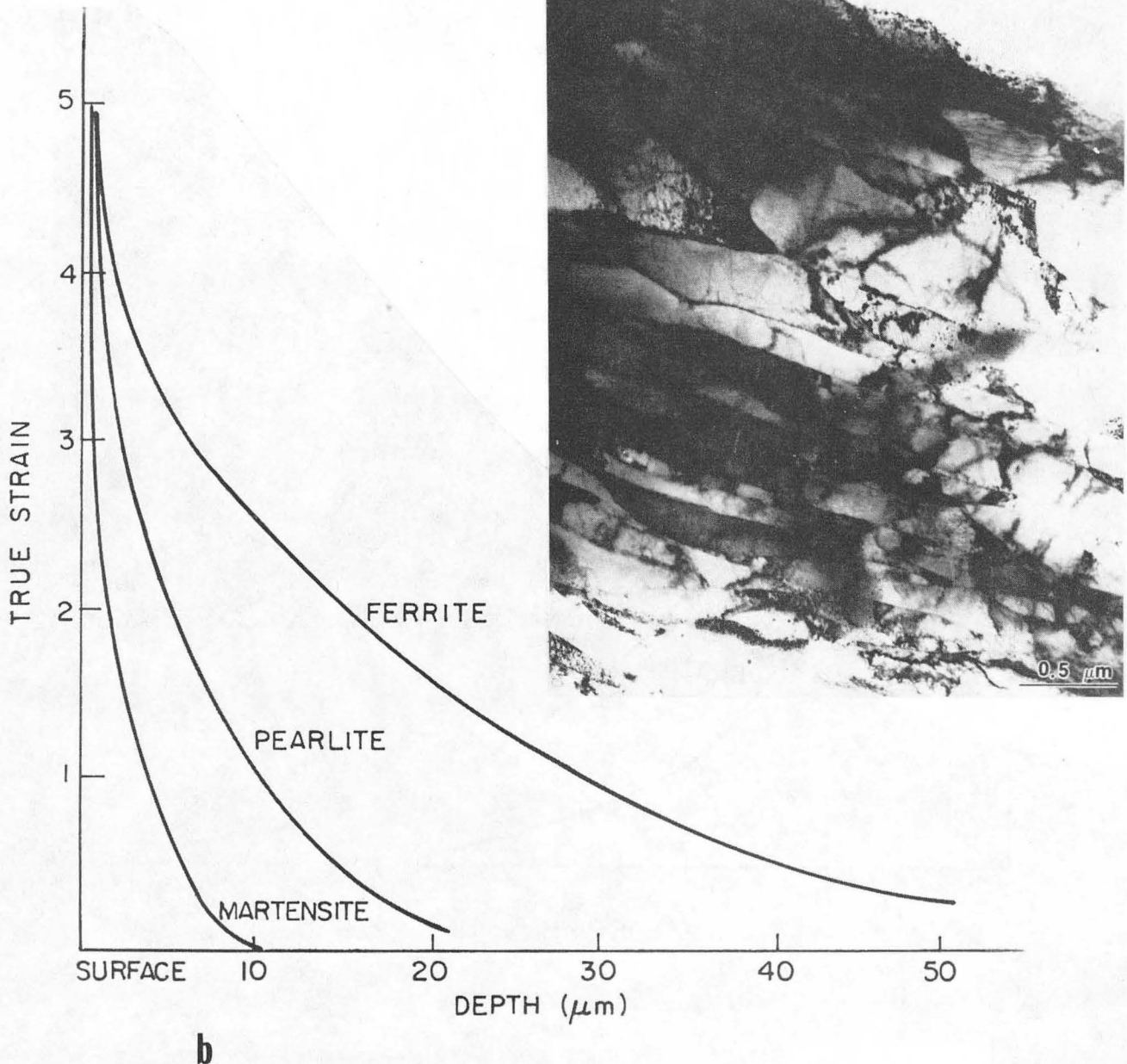
PEARLITE 1020 STEEL



XBB 827-5917A

Figure 9: Strain distribution in 1020 steel as a function of distance beneath the wear surface. a) Strain distribution from distortion of pearlite colonies. Inset shows representative area from aligned pearlite. Near surface strains are indeterminate. b) Strain distribution derived from dislocation cell size measurements. Inset is representative of a dislocation structure 2.0-6.0 microns from the interface

SUBSURFACE STRAIN
2 Kg LOAD



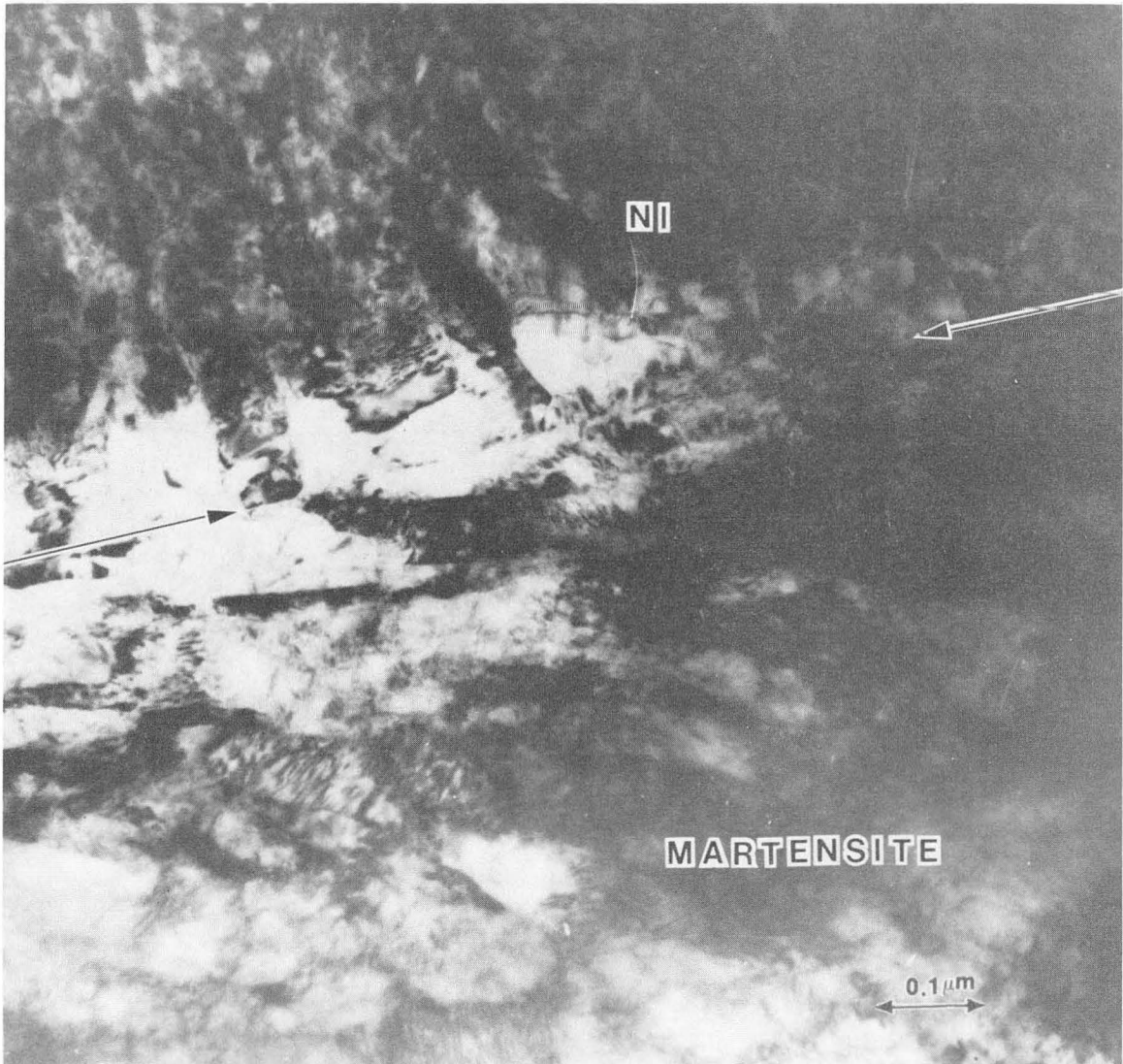
XBB 823-2868A

Figure 9: Strain distribution in 1020 steel as a function of distance beneath the wear surface. a) Strain distribution from distortion of pearlite colonies. Inset shows representative area from aligned pearlite. Near surface strains are indeterminate. b) Strain distribution derived from dislocation cell size measurements. Inset is representative of a dislocation structure 2.0-6.0 microns from the interface



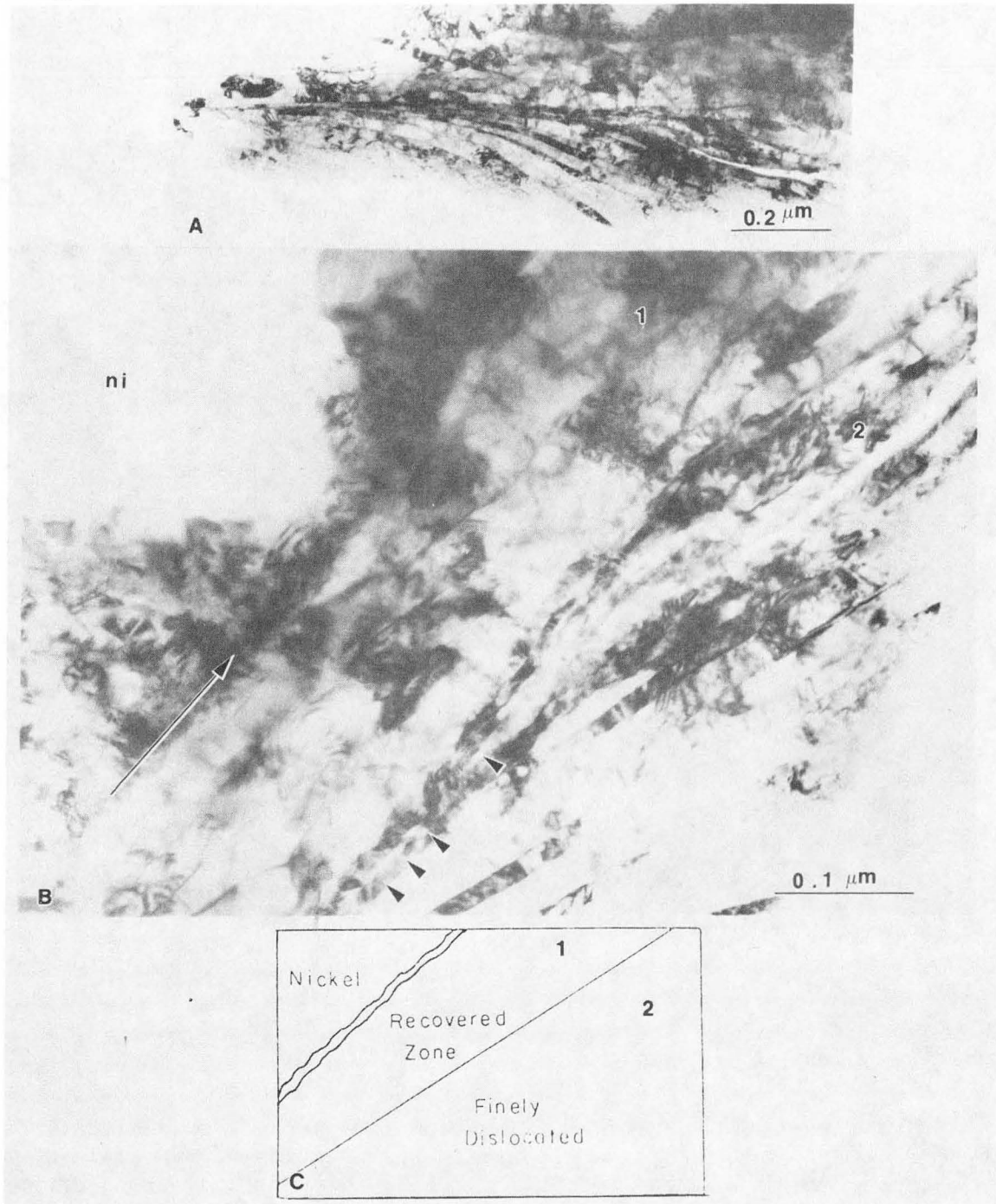
XBB 819-11945

Figure 10: TEM micrograph. Longitudinal cross section of ferritic iron reveals the characteristic dislocation cell structure. Arrow indicates the direction of sliding.



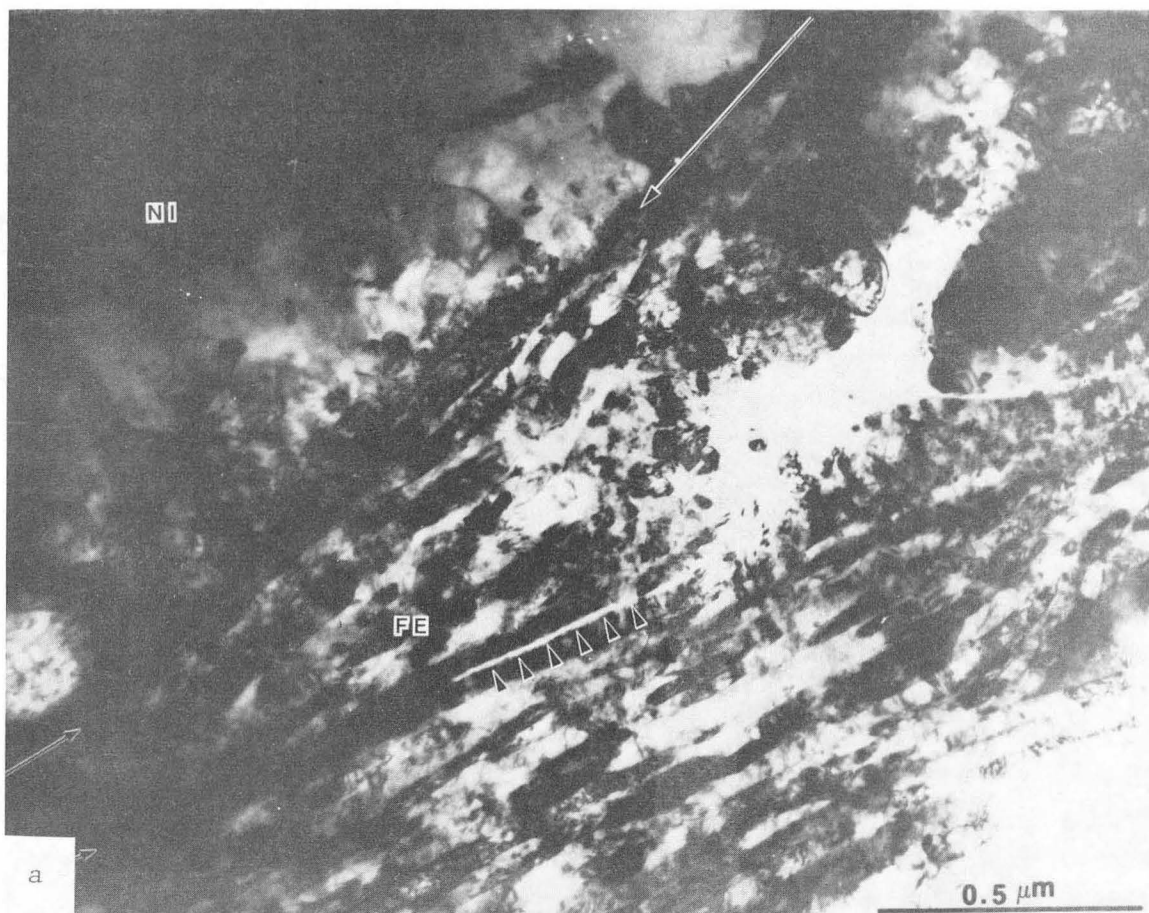
XBB 827-5916A

Figure 11: TEM micrograph of longitudinal cross-section of martensitic steel. Sliding direction is from right to left. Arrows denote the wear interface where martensite laths appear to have necked down 100% from their original size.



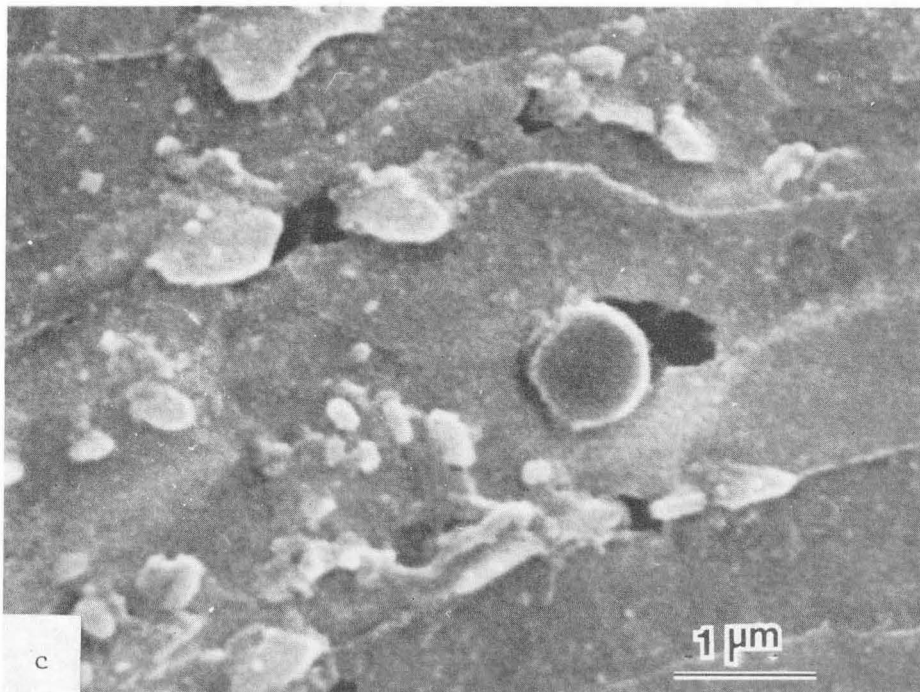
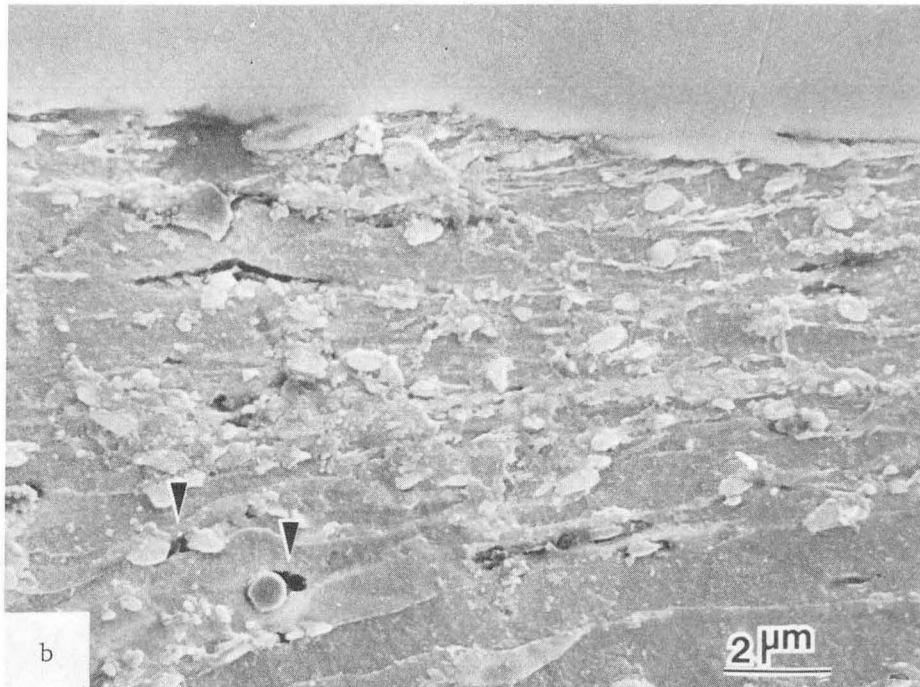
XBB 823-2869

Figure 12: TEM micrograph of longitudinal cross-section of pearlitic steel. a) Low magnification of the interface region. Arrows denote the wear interface b) Enlargement of (a) showing coarser cell structure indicating recovery below the interface. The heavily dislocated fine cell structure is below. Cracks are indicated at the junction of these regions. c) Schematic diagram of the micrograph in (b)



XBB 821-895A

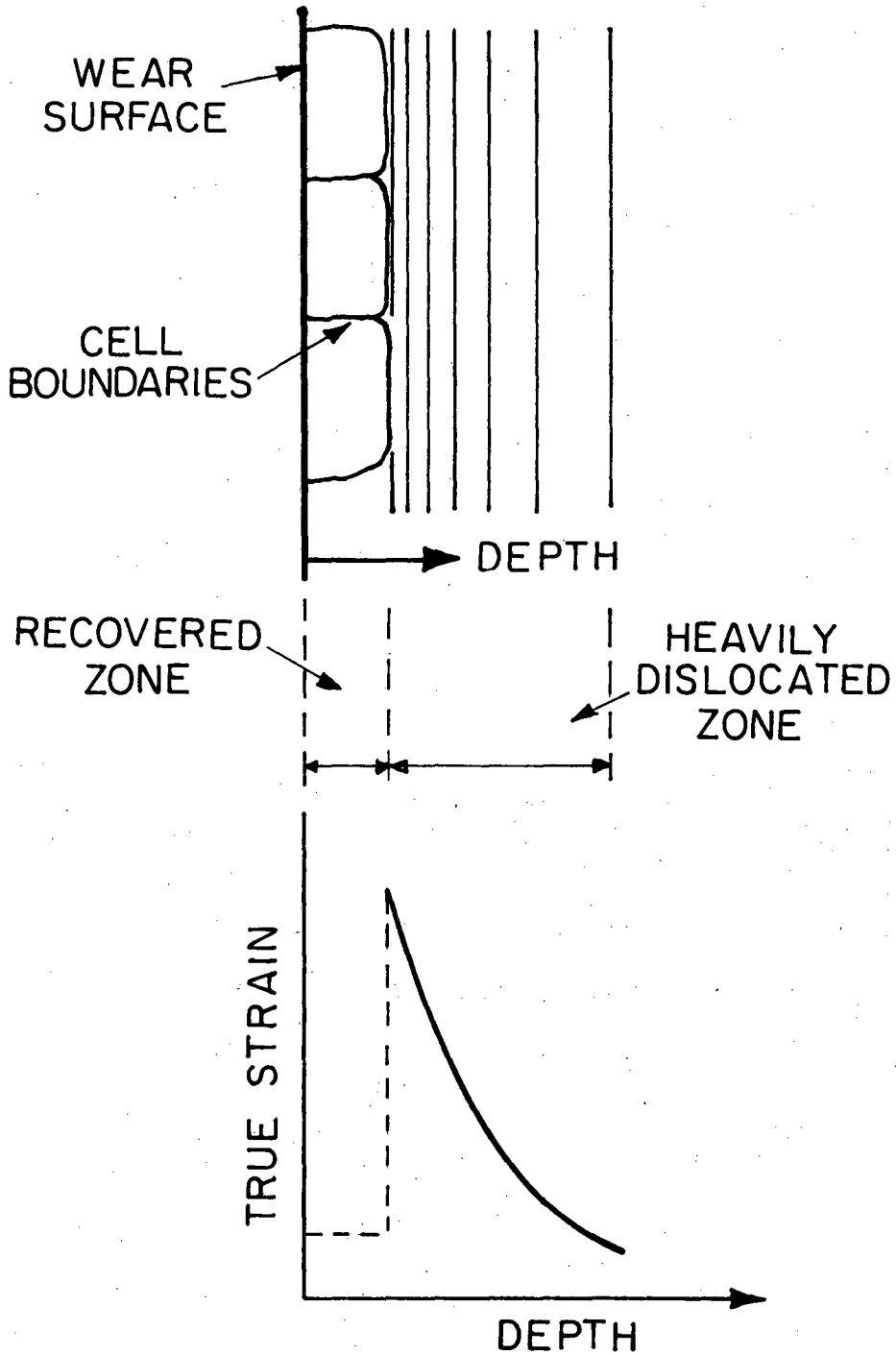
Figure 13: a) Crack initiation associated with dislocations. TEM micrograph. Longitudinal cross section of pearlitic steel, showing apparent formation of a debris particle. Long arrows indicate the Fe-Ni interface. b)c) Crack initiation and decohesion (arrowed) associated with carbides.



XBB 826-5045

Figure 13: a) Crack initiation associated with dislocations. TEM micrograph. Longitudinal cross section of pearlitic steel, showing apparent formation of a debris particle. Long arrows indicate the Fe-Ni interface. b)c) Crack initiation and decohesion (arrowed) associated with carbides.

STRAIN GRADIENT



XBL 829-6465

Figure 14: Schematic representation of shear strain gradient generated in close proximity to wear surface

CRACK INITIATION MECHANISMS

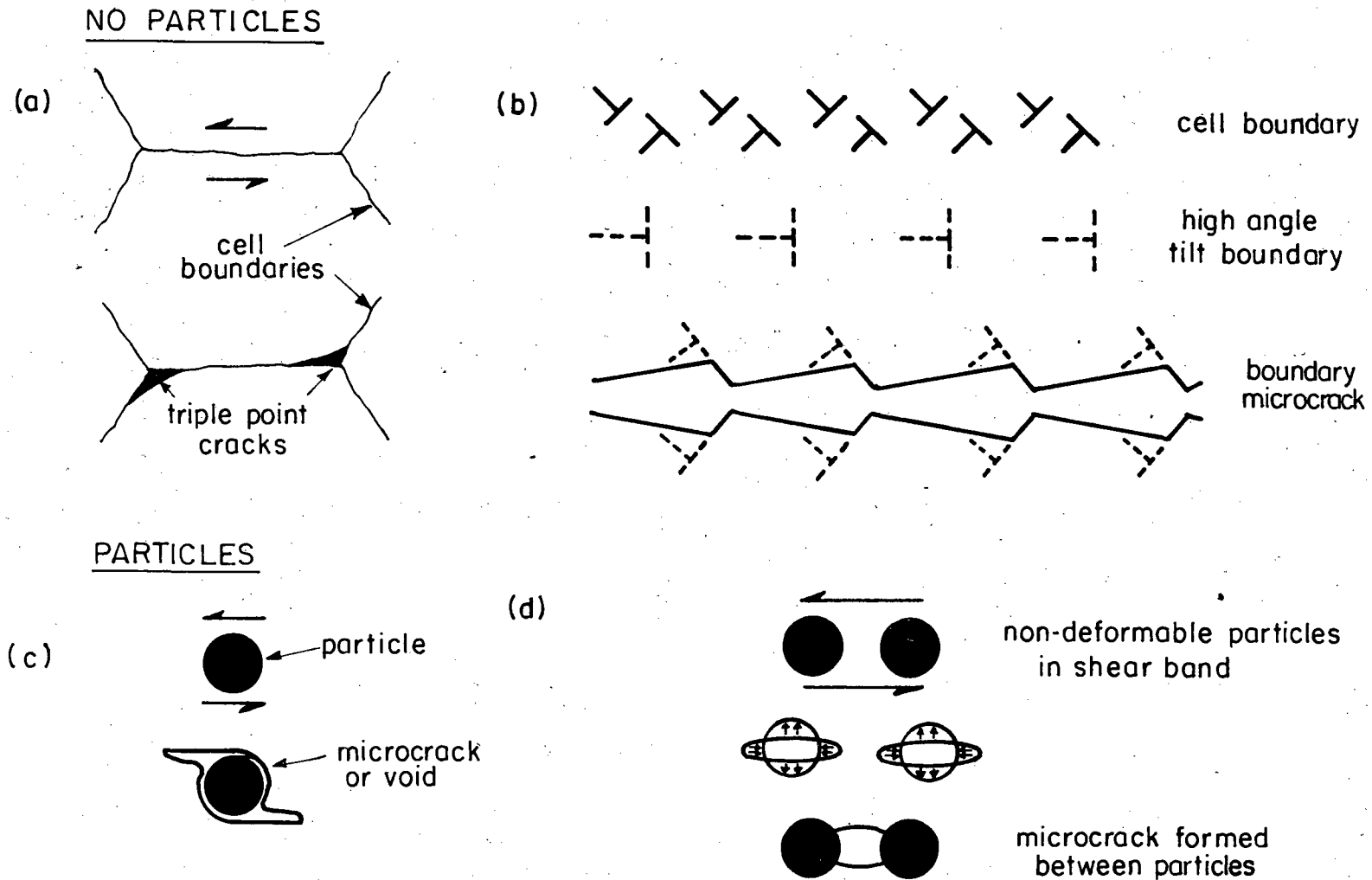
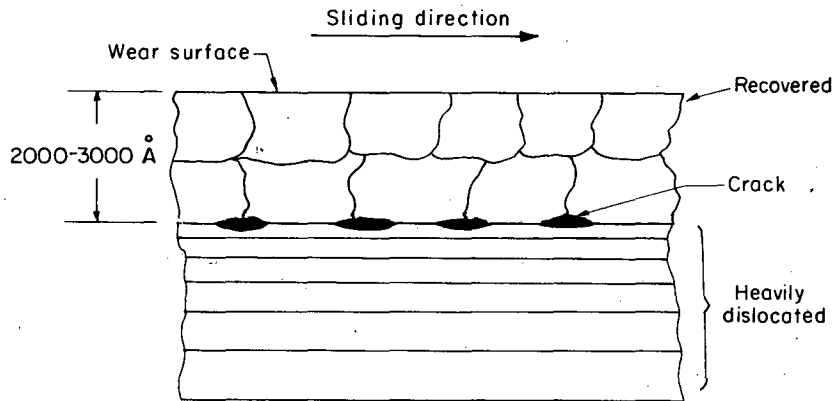
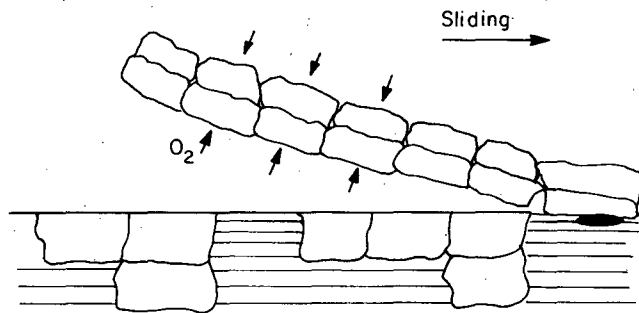


Figure 15: Mechanisms of sub-surface initiation of wear cracks, a) b) for microstructures containing no particles where cracks preferentially nucleate within the cell boundaries at the interface between the heavily dislocated and recovered pores, and c) d) for microstructures containing particles where cracks preferentially nucleate at the particle interfaces.

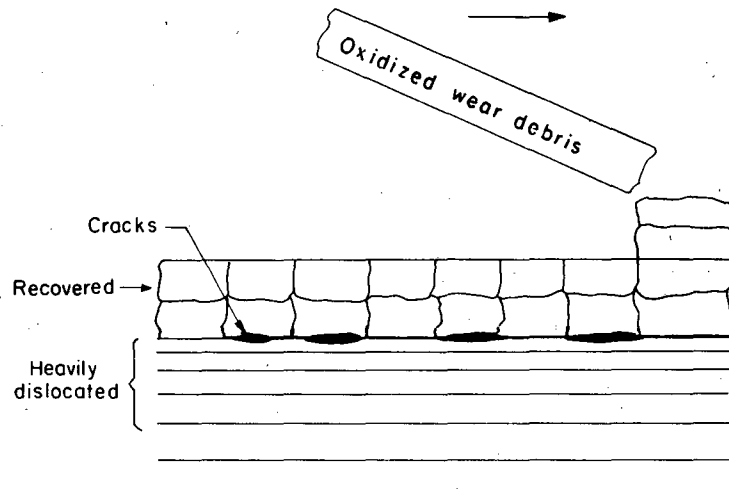
Step A



Step B Wear particle in process of formation.



Step C



XBL 824-5509

Figure 16: Schematic overview of the unlubricated sliding wear process.

This report was done with support from the Department of Energy. Any conclusions or opinions expressed in this report represent solely those of the author(s) and not necessarily those of The Regents of the University of California, the Lawrence Berkeley Laboratory or the Department of Energy.

Reference to a company or product name does not imply approval or recommendation of the product by the University of California or the U.S. Department of Energy to the exclusion of others that may be suitable.

TECHNICAL INFORMATION DEPARTMENT
LAWRENCE BERKELEY LABORATORY
UNIVERSITY OF CALIFORNIA
BERKELEY, CALIFORNIA 94720